

PAPER • OPEN ACCESS

High voltage flexible glucose/O₂ fully printed hydrogel-based enzymatic fuel cell

To cite this article: Verdiana Marchianò *et al* 2024 *J. Phys. D: Appl. Phys.* **57** 135503

View the [article online](#) for updates and enhancements.

You may also like

- [Modeling net effects of transit operations on vehicle miles traveled, fuel consumption, carbon dioxide, and criteria air pollutant emissions in a mid-size US metro area: findings from Salt Lake City, UT](#)
Daniel L Mendoza, Martin P Buchert and John C Lin
- [Band gap properties and self-collimation in a tenfold quasicrystal structure photonic crystals applying multicircular ring scatterers](#)
Yang Zhou, Zhi-Ran Zhang, Hui Ji et al.
- [Toroidal modeling of the \$n = 1\$ intrinsic error field correction experiments in EAST](#)
Xu Yang, Yueqiang Liu, Youwen Sun et al.

PRIME
PACIFIC RIM MEETING
ON ELECTROCHEMICAL
AND SOLID STATE SCIENCE








HONOLULU, HI
Oct 6–11, 2024

Abstract submission deadline:
April 12, 2024

Learn more and submit!

Joint Meeting of
The Electrochemical Society
•
The Electrochemical Society of Japan
•
Korea Electrochemical Society

High voltage flexible glucose/O₂ fully printed hydrogel-based enzymatic fuel cell

Verdiana Marchianò^{1,2,7} , Angelo Tricase^{1,2,7} , Nicoletta Ditaranto^{1,2} ,
Eleonora Macchia^{2,3,4} , Silvia d'Ingeo^{1,3}, Cinzia Di Franco⁵ , Gaetano Scamarcio^{5,6} ,
Luisa Torsi^{1,2,*}  and Paolo Bollella^{1,2,*}

¹ Dipartimento di Chimica, Università degli Studi di Bari Aldo Moro, Bari 70125, Italy

² Centre for Colloid and Surface Science, Università degli Studi di Bari Aldo Moro, 70125 Bari, Italy

³ Dipartimento di Farmacia—Scienze del Farmaco, Università degli Studi di Bari Aldo Moro, Bari 70125, Italy

⁴ Faculty of Science and Engineering, Åbo Akademi University, 20500 Turku, Finland

⁵ Istituto di Fotonica e Nanotecnologie CNR, c/o Dipartimento Interateneo di Fisica, Università degli Studi di Bari Aldo Moro, Bari 70125, Italy

⁶ Dipartimento Interateneo di Fisica, Università degli Studi di Bari Aldo Moro, Bari 70125, Italy

E-mail: luisa.torsi@uniba.it and paolo.bollella@uniba.it

Received 15 July 2023, revised 28 November 2023

Accepted for publication 22 December 2023

Published 4 January 2024



CrossMark

Abstract

Herein we report on a novel enzymatic fuel cell (EFC) based on stencil printed electrodes modified with pyrrolo quinoline quinone glucose dehydrogenase and bilirubin oxidase, which are assembled by considering two different configurations: (i) normal assembling in liquid electrolyte and (ii) six EFCs connected in series, each one comprising both bioanode and biocathode, coupled through a hydrogel-based electrolyte in a stack-like mode similar to a Voltaic pile. After a deep electrodes characterization, they are assembled according to the first configuration obtaining an open circuit voltage (OCV) of 0.562 ± 0.002 V. Moreover, the EFC performance are substantially improved by using the second configuration (six EFCs connected in series) obtaining an OCV of 2.36 ± 0.22 V with a maximum power output of $22.9 \pm 0.9 \mu\text{W}$ at a cell voltage of 1.95 V (operating in 10 mM D-glucose). This innovative approach represents a proof-of-concept towards the development of renewable power sources and could serve as a critical step in powering implantable bioelectronics, such as pacemakers.

Supplementary material for this article is available [online](#)

Keywords: water-based conductive inks, modified electrodes, enzymatic fuel cell, glucose biosensors, hydrogel-based electrolyte

⁷ These authors contributed equally to this work.

* Authors to whom any correspondence should be addressed.



Original content from this work may be used under the terms of the [Creative Commons Attribution 4.0 licence](#). Any further distribution of this work must maintain attribution to the author(s) and the title of the work, journal citation and DOI.

1. Introduction

Recently, most of the research on enzymatic fuel cells (EFCs) has been focused on tailoring/coupling anodic enzymes, able to oxidize a fuel as source of electrons (*e.g.* glucose dehydrogenase, glucose oxidase (GOx), lactate oxidase, lactate dehydrogenase *etc.*), with cathodic enzymes, typically able to reduce oxygen (oxygen reduction reaction, ORR) to water, like laccase or bilirubin oxidase (BOx) [1–5].

Particularly, many examples of implanted EFCs attempting energy harnessing from blood or other bodily fluids (as source of glucose) have been investigated to power low energy demanding electronic devices (*e.g.* insulin pumps, pacemakers, capacitors *etc.*) [3, 6–8]. This represented a key achievement towards standalone devices that could revolutionize the development of Point-of-Care (PoC)/Point-of-Need (PoN) devices making them available in remote area of the World [9]. However, since 1970s, it was clear that the power/energy density supplied by EFCs could not be comparable with traditional batteries or fuel cells (FCs), hence not able to power high energy demanding devices like smartphones or computers [10]. Moreover, EFCs also addressed biotechnologist/biochemists towards enzyme engineering to enlarge the library of enzymes (wild type or mutant) able to perform/improve direct electron transfer (DET) between redox centers and electrodes, minimizing their O₂ responsiveness (O₂ is the natural electron acceptor in many biological processes) [4, 11]. Since PQQ-GDH exhibits reduced substrate specificity and decreased stability compared to GOx, many protein engineers focused on improving its properties towards biosensors and EFCs development [12].

There are also other technological constrains at EFCs development such as limited open-circuit voltage (OCV) and limited energy density supplied [3]. In these regards, novel printing technologies (*e.g.* stencil-printing, screen-printing, ink-jet printing, 3D-printing, and laser printing *etc.*) and series cells stacking can tackle these issues [13–15]. In all printing technologies, ink formulation plays a key role particularly considering both rheological properties (viscosity, shear-thinning) and electrochemical properties (electroactive area, roughness factor) [16–19]. In addition, most of the aforementioned printing technologies require post-production modifications like atomic layer deposition or electrodeposition, electrochemical polishing, solvent activation, enzyme activation, thermal activation, *etc.* while stencil-printing offers a cost effective and easy end-user fabrication alternative without any post-production process considering the possibility of integrating enzymes already within the conductive ink [20–22].

Recently, there has been an increasing interest towards water-based conductive inks especially due to their lower cost, higher conductivity and room temperature curing procedures compared to traditional organic solvents-based conductive inks [23, 24]. The latter exhibit low conductivity and poison proteins, hence hindering their utilization for electrode manufacturing [19]. Reproducibility and operational stability represent the challenge for the development of wearable technologies including biosensors and EFCs [9]. In this regard, the

enzymes integration within conductive inks can be a solution to improve reproducibility, operational stability, storage stability, stiffness, and robustness of electrodes for EFCs and biosensing [25, 26].

For *in vivo* applications, sterilization, preventing blood clots (*i.e.* electrode treatment with heparin), biocompatibility and lifetime should be accounted. This will be a key step towards implantable biofuel cells [27].

Furthermore, hydrogel-based electrolytes have been considered for developing several electrochemical devices [28, 29]. Despite their high ionic conductivity, liquid electrolytes can be dangerous for batteries construction considering uneven spill of concentrated inorganic salts solution (acidic/basic electrolytes), spill of organic solvents, low electrochemical stabilities (limited voltage range due to H₂O oxidation/reduction) and low miniaturization [30, 31]. All these issues hinder their possibility to power miniaturized/wearable bioelectronics, often in direct contact with bodily fluids. Conversely, hydrogel-based electrolytes, despite their lower ionic conductivity, can be exploited to develop flexible, stretchable, and wearable electronics (*e.g.* self-powered biosensors, biosupercapacitors, actuators *etc.*) [32].

Moreover, hydrogel-based electrolytes offer enhanced safety and adaptability when compared to traditional liquid electrolytes in flexible energy storage devices. They also have the potential to enhance the electrochemical performance of these devices. In addition to these advantages, hydrogel electrolytes can be engineered to possess self-protective, thermotolerant, self-healing, and other desirable properties, contributing to their rapidly advancing development [28, 33, 34].

Nishizawa and colleagues, for instance, utilized an agarose hydrogel as both the electrolyte and fuel retainer in a flexible w-BFC (wearable biofuel cell). They combined a multi-walled carbon nanotube (MWCNTs)-modified carbon fiber (CF) anode with immobilized D-FDH (fructose dehydrogenase) and a MWCNT-CF cathode with immobilized BOD (BOx) to assemble the biofuel cell. Impressively, this configuration achieved a maximum power density of 550 $\mu\text{W cm}^{-2}$ at 0.4 V, maintaining its performance even when the biofuel cell was bent to an angle of 44 degrees.

EFCs rely on redox enzymes that catalyze oxidation of electron donors and reduction of oxidants like molecular oxygen [26, 35, 36]. Despite their wide employment both as biosensors or EFCs anode, oxidases do not represent the ‘ideal’ candidates for electrode construction because they are unable to transfer electrons directly to the electrode requiring natural or artificial electron acceptors/shuttles [37]. In particular, O₂ is reduced to H₂O₂ that can diffuse towards the cathodic electrode causing its poisoning and EFCs performance worsening. On the other hand, artificial electron acceptors/shuttles need to be properly selected to minimize the thermodynamic barrier of the electron transfer process between the enzymatic redox center and the electrodes [38, 39]. Pyrroloquinoline quinone (PQQ)-dependent glucose

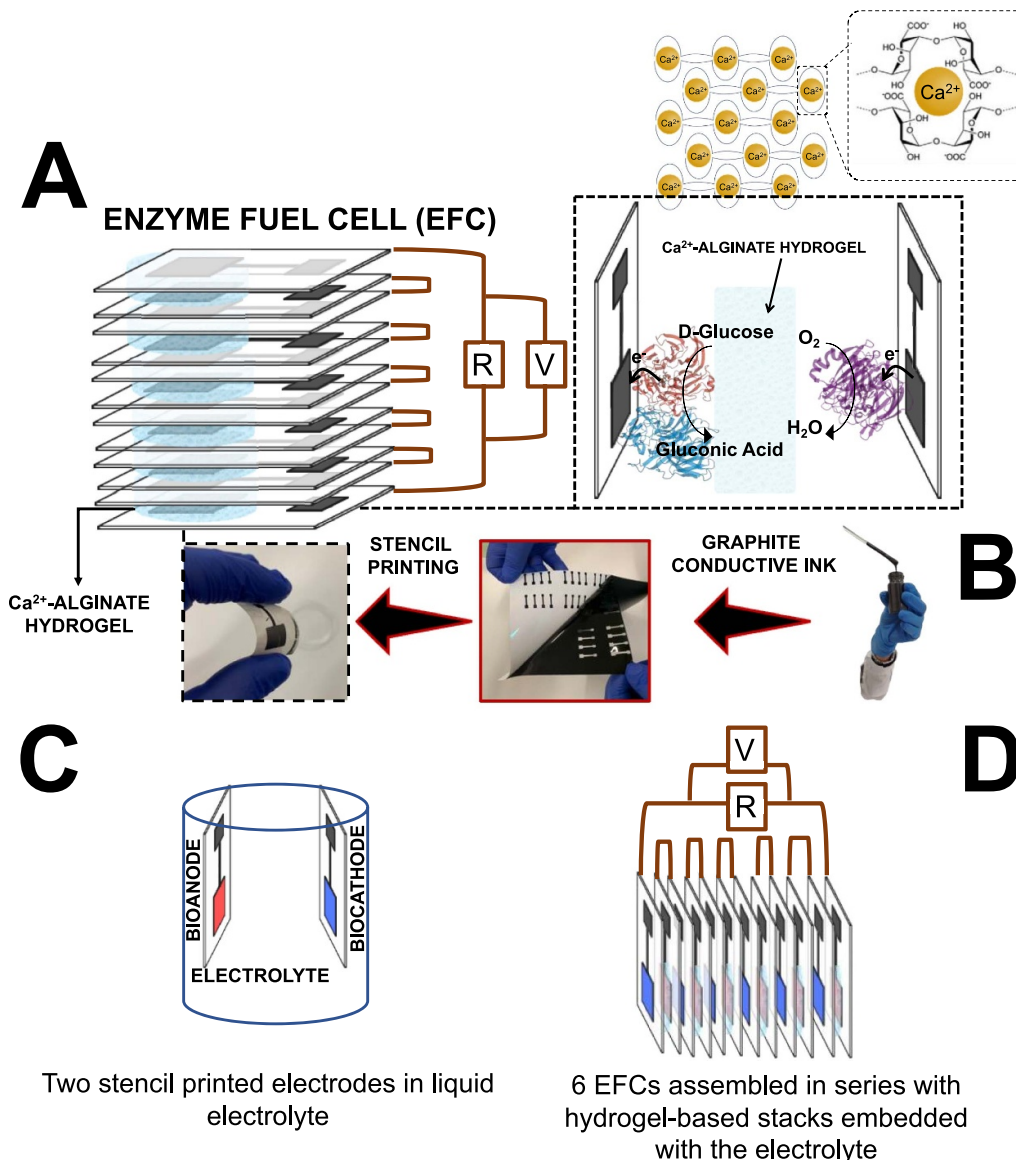


Figure 1. (A) Scheme of the high voltage flexible glucose/O₂ fully printed hydrogel-based electrolyte enzymatic fuel cell. The electrodes are modified with PQQ-glucose dehydrogenase and bilirubin oxidase and stacked with Ca²⁺-alginate hydrogel (inset: egg-box structure); (B) the graphite modified electrodes are prepared by stencil-printing from water-based graphite conductive ink previously formulated; (C) configuration (i) two stencil printed electrodes and (D) configuration (ii) 6 EFCs assembled in series with hydrogel-based stacks embedded with the electrolyte.

dehydrogenase (PQQ-GDH) represents a valid alternative being oxygen insensitive and able to transfer electrons directly to the electrode [12]. Notably, BOx from *Myrothecium verrucaria* (*Mv*BOx) has been widely employed as cathodic electrode to conceive EFCs working at human physiological pH. BOx catalyzes a 4e⁻/4H⁺ reduction of O₂ to H₂O with a low overpotential, being its formal potential (E^{0'}) close to the thermodynamic O₂/H₂O redox potential (*i.e.* +0.69 V vs. SCE) [40].

This work reports a novel fully printed EFCs with hydrogel-based electrolyte to maximize the OCV and power output (*P*_{out}) as reported in figure 1(A). Figure 1(B) shows

schematically the water-based carbon ink formulation to print flexible electrodes by stencil-printing (SPG) and the connection in series of six EFCs (smaller than AAA battery) encompassing a bioanode based on PQQ-GDH catalyzing glucose oxidation and a biocathode based on *Mv*BOx catalyzing O₂ reduction. Both the electrodes and the hydrogel were characterized through electrochemical measurements (electroactive area, electron transfer rate constant, electrochemical impedance spectroscopy (EIS)), spectroscopic and morphological measurements to optimize the EFCs assembling. Finally, the device was assembled and tested including in a model solution (10 mM D-glucose) within the hydrogel.

2. Experimental

2.1. Chemicals and reagents

4-(2-Hydroxyethyl)piperazine-1-ethanesulfonic acid (HEPES), 4-Morpholinepropanesulfonic acid (MOPS), acetic acid (CH_3COOH), alginate sodium salt from brown algae (medium viscosity), bovine serum albumin (BSA), D-glucose, D-galactose, D-mannitol, L-lactic acid, potassium chloride (KCl), calcium chloride (CaCl_2), potassium ferri-cyanide ($\text{K}_3\text{Fe}(\text{CN})_6$), potassium ferrocyanide ($\text{K}_4\text{Fe}(\text{CN})_6$), hydrochloric acid (HCl), potassium hydroxide (KOH), sodium acetate (CH_3COONa), sodium hydroxide (NaOH), ascorbic acid, D-fructose, dopamine hydrochloride, isopropyl alcohol (IPA), graphite powder ($<20\ \mu\text{m}$, synthetic), chitosan medium molecular weight, glycerol (ACS grade $\geq 99.5\%$) and uric acid were purchased from Merck Millipore (formerly Sigma Aldrich).

Pyrolo quinoline quinone glucose dehydrogenase (PQQ-GDH) was obtained from Toyobo Enzymes. The PQQ-GDH (activity $787\ \text{U ml}^{-1}$) was dissolved in 10 mM HEPES buffer at pH 7.4 containing 6 mM CaCl_2 (stored in aliquots at $-20\ ^\circ\text{C}$). BOx from *Myrothecium verrucaria* was kindly provided by Amano Enzyme. BOx (activity $38\ \text{U ml}^{-1}$), dissolved in 20 mM TRIS buffer pH 8 containing 100 mM Na_2SO_4 (stored in aliquots at $-20\ ^\circ\text{C}$) [36].

All solutions were prepared using Milli-Q water ($18.2\ \text{m}\Omega\ \text{cm}$, Millipore, Bedford, MA, USA).

2.2. Electrode preparation and modification

The water-based conductive ink was formulated using graphite, chitosan, and glycerol [19]. Graphite served as the conductive material, chitosan as the binder, and glycerol as the stabilizer. A 2.5% w/v chitosan solution was prepared by dissolving chitosan in 1 M acetic acid. The solution was stirred at room temperature overnight. Subsequently, the chitosan solution was diluted to a final concentration of 1% w/v with distilled water, resulting in an acetic acid concentration of 0.4 M.

To prepare the conductive ink, 5 g of graphite powder was mixed with 10 ml of the previously prepared chitosan solution, along with 500 μl of glycerol.

The SPG electrodes were prepared using polyethylene terephthalate (PET) sheets. The sheets were cleaned three times with IPA and distilled water, and then sanded with fine emery paper (1500 grit) to enhance the adhesion of the ink. A stencil was created on a Smart Vinyl adhesive sheet using a Circuit Explore[®] 3 machine equipped with Design Space Software v.7.3.95. The stencil was applied onto the PET sheet, and 500 μl of the conductive ink was placed on the PET sheet and spread using a scrape. The prepared electrode was allowed to dry at room temperature for 10 min and then cured in an oven at $100\ ^\circ\text{C}$ for 1 min. Afterward, the stencil was peeled off, and the connecting track between the working electrode and the pad was insulated using nail polish.

The bioanode was prepared by drop-casting 5 μl of PQQ-GDH solution (dissolved in 10 mM HEPES buffer at pH 7.4 containing 6 mM CaCl_2 and 1 mg ml^{-1} BSA, activity $787\ \text{U ml}^{-1}$). Similarly, the biocathode was prepared by drop-casting 5 μl of BOx solution (dissolved in 20 mM TRIS buffer pH 8 containing 100 mM Na_2SO_4 and 1 mg ml^{-1} BSA, activity $38\ \text{U ml}^{-1}$). The electrodes were further conditioned overnight in 10 mM HEPES buffer pH 7.2 at $+4\ ^\circ\text{C}$.

2.3. Hydrogel-based electrolyte

To prepare the hydrogel beads, sodium alginate was dissolved in water and stirred overnight at $30\ ^\circ\text{C}$ until achieving a final concentration of 2% w/v [41, 42]. The alginate solution containing the protein was then added drop by drop to a 20 mM aqueous solution of CaCl_2 . As a result, millimeter-sized hydrogel beads were formed through the crosslinking reaction between the alginate and calcium ions present in the CaCl_2 solution. The beads were allowed to mature for 15 min in the CaCl_2 solution, during which further crosslinking occurred and the beads achieved their final stability and shape. Finally, the beads were cut to achieve the disk shape with an optimized thickness of 2 mm, figure S1 (supporting information). The Ca^{2+} -crosslinked alginate hydrogel layer was frozen in liquid N_2 and immediately dried under vacuum overnight. Imaging was performed in the center and the edger part of the layer.

2.4. EFC assembly

The EFC was assembled according to two different configurations for PQQ-GDH bioanode and BOx biocathode: (i) two stencil printed electrodes in liquid electrolyte; (ii) six EFCs assembled in series with hydrogel-based stacks embedded with the electrolyte, as shown in figures 1(C) and (D), respectively. Finally, the EFC setups were tested in a model solution (10 mM D-glucose in 10 mM HEPES buffer pH 7.5).

2.5. Electrochemical measurements

Cyclic voltammetry (CV), EIS and amperometry experiments were performed using a PalmSens4 electrochemical workstation equipped with PSTrace 5.6 v software. All potentials were measured using a BASi Ag/AgCl/KCl, 3 M (all potential values reported in the paper need to be considered toward this reference) and a platinum wire as reference and counter electrode, respectively. SPG electrodes (geometric area = $1\ \text{cm}^2$) were used as working electrodes. Polarization curves were recorded using linear sweep voltammetry in potentiostatic mode at a scan rate of $1\ \text{mV s}^{-1}$, ranging from the OCV to 0 V. The bioanode, PQQ-GDH/SPG, was employed as the working electrode, while BOx/SPG served as a combined reference and counter electrode. In the first assembly mode, both biocomponents were placed in an electrochemical cell without the use of a proton-exchange membrane. The experimental setup included 10 mM glucose in a 10 mM HEPES buffer at pH 7.5.

In the second assembly mode, the six EFCs were connected in series using hydrogel stacks. These hydrogel stacks contained 10 mM glucose in a 10 mM HEPES buffer at pH 7.5. The temperature-controlled experiments were conducted using a cryostatic bath (LAUDA RM6, Delran, NJ, USA) with a precision of ± 0.01 °C.

2.6. Morphological and spectroscopic characterization

The morphological characterization was conducted using a field emission scanning electron microscope (FE-SEM) model Sigma Zeiss (Jena, Germany). Images were acquired in top-view using the in-lens detector, with a 5 KV acceleration voltage, 4 mm working distance, 30 μm opening, and no additional sample treatment.

X-ray photoelectron spectroscopy (XPS) analyses were performed using a Versa Probe II Scanning XPS spectrometer from Physical Electronics GmbH. The instrument was equipped with an AlK α source, and the spot size was set to 200 μm . Wide-scan and high-resolution spectra were obtained in CAE mode, with a pass energy of 117.40 eV and 29.35 eV, respectively. The source power was set to 49.2 W. To compensate for sample charging, an electron gun operating at 1.0 V and 20.0 μA was utilized. The acquired data were analyzed using the MultiPak v. 9.9.0.8 software.

3. Results and discussion

3.1. Electrochemical, spectroscopic and morphological characterization of printed electrodes

Graphite printed electrodes were prepared as previously described by stencil-printing of water-based graphite conductive ink onto flexible PET.

The electrodes were preliminarily characterized by CV in 5 mM Fe(CN) $_6^{3-/4-}$, at different scan rates (5–150 mV s^{-1}), as shown in figure 2(A). SPG electrodes displayed a peak-to-peak separation of 0.228 V at 50 mV s^{-1} and an electroactive area (A_{EA}) of 4.05 ± 0.4 cm^2 (calculated according to Randles–Ševčík equation, figure 2(A) inset), hence a roughness factor (ρ) of 4.05 (considering a geometric area ($A_{\text{GEO}} = 1$ cm^2)). Moreover, the electron transfer rate efficiency has been evaluated accounting for a mixed model based on an extended method merging the Klingler-Kochi and Nicholson and Shain methods that could be applied either to completely irreversible or reversible systems [43]. The electron transfer rate constant (k^0) was $(9.3 \pm 0.6) \times 10^{-3}$ cm s^{-1} . SPG electrodes were further characterized by using EIS in ferri/ferrocyanide solution and applying a Ca $^{2+}$ cross-linked alginate hydrogel containing the redox probe to investigate the resistance to the charge transfer (R_{CT}), as reported in figure 2(B). In particular, SPG electrodes exhibited an R_{CT} of $(2.969 \pm 0.041) \times 10^3$ Ω in ferri/ferrocyanide solution, which is in good agreement with the literature [22], and R_{CT} of $(2.947 \pm 0.536) \times 10^4$ Ω applying a Ca $^{2+}$ cross-linked alginate hydrogel containing ferri/ferrocyanide solution. The R_{CT} difference can be certainly ascribed to a different

ionic conductivity between the electrolyte solution, typically 1.15 S cm^{-1} (10 mM HEPES buffer containing 100 mM KCl (as supporting electrolyte)), and 0.027 S cm^{-1} for Ca $^{2+}$ cross-linked alginate hydrogel, as reported in the literature [44].

The specific capacitance of the electrode at various scan rates were calculated basing on the CV curves according to the following equation:

$$C = \left(\int IdV \right) / mvV \quad (1)$$

where I is the response current density (A g^{-1}), V is the potential (V), v the potential scan rate (V s^{-1}), and m is the mass of the active material in the electrode (g) [45]. Figure 2(C) reports CV curves in 10 mM HEPES buffer pH 7.2 + 100 mM KCl at different scan rates, but the CV curve at 5 mV s^{-1} was used to calculate the specific capacitance, resulting to be 158 ± 7 F g^{-1} . The CV shape of bare SPG was nearly rectangular, which indicated that the sample had good conductivity and was close to ideal electric double-layer capacitors (EDLC). When the scan rate increased to 300 mV s^{-1} , the curve shape still maintained nearly rectangular, which indicated bare SPG played superior capacitive performance even at high current density and signified good electrochemical performance as an EDLC electrode material. The resulting EFC can behave as a supercapacitor being able to store the charge derived by oxidation/reduction process catalyzed by the enzymes immobilized onto the current collector.

The SPG electrodes characterized by SEM display a rough surface (figure 2(D)), confirming the high roughness factor of these electrodes. The surface chemical composition analysis of the electrodes was performed by using XPS to investigate the influence of curing time (0–180 s) at fixed temperature and temperature effect (room temperature–180 °C) at fixed curing time, as shown in figure 2(E). From the line shape of C1s spectral region it was possible to observe the overlapping of all the spectra, demonstrating that both the curing time and the temperature do not induce any oxidation/degradation of the electrodes surface.

3.2. Bioelectrocatalytic characterization of PQQ-GDH/SPG electrode

To assess the catalytic behavior of modified anode electrode, notably SPG with physisorbed PQQ-GDH, several CVs experiments in 10 mM HEPES buffer pH 7.5 + 100 mM NaClO $_4$ by adding 10 mM D-glucose as substrate. The same experiments were performed by using Ca $^{2+}$ cross-linked alginate hydrogel containing testing solution.

Figure 3(A) shows the CVs in the absence (black curve) and presence of 10 mM D-glucose (red curve). In non-turnover conditions, PQQ-GDH/SPG electrodes did not show any redox peak eventually correlated with non-turnover redox activity. After substrate addition, a catalytic curve starting at $E_{\text{ONSET}} = -0.065$ V with maximum current of 13 μA at $E = 0.4$ V (figure 3(A), red curve) was observed. Similarly, PQQ-GDH/SPG electrodes were tested by using

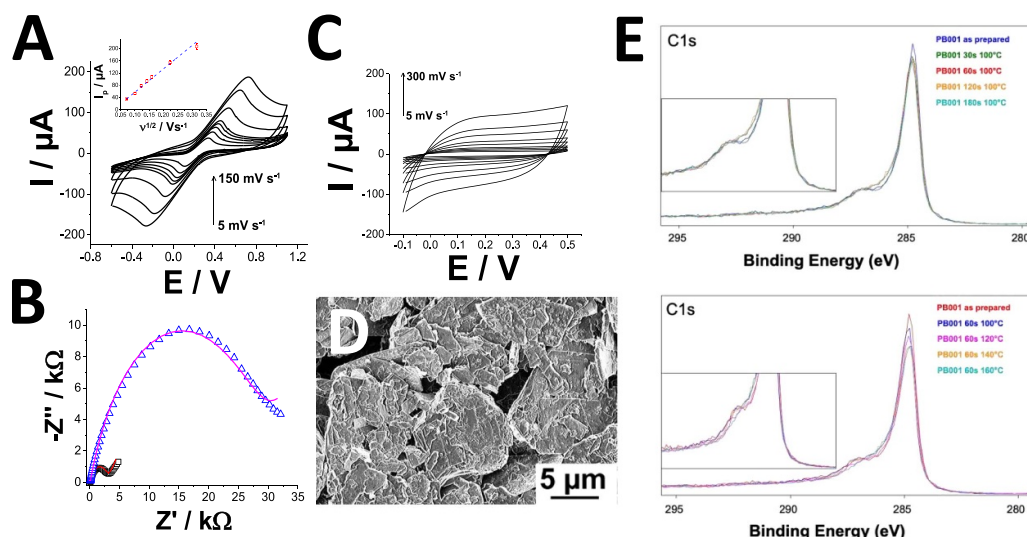


Figure 2. (A) CVs at different scan rates of SPG electrode recorded in 5 mM $\text{Fe}(\text{CN})_6^{3-/4-}$ (prepared in 10 mM HEPES buffer pH 7.5 + 100 mM KCl) and slope i_p vs. $v^{1/2}$ (inset); (B) EIS curve measured at $E = 0.23$ V between 100 000 and 0.1 Hz in 5 mM $\text{Fe}(\text{CN})_6^{3-/4-}$ (prepared in 10 mM HEPES buffer pH 7.2 + 100 mM KCl) for SPG in liquid electrolyte (black dots, fitted red curve) and SPG in hydrogel-based electrolyte (blue dots, fitted magenta curve); (C) CVs at different scan rates of SPG electrode recorded in 10 mM HEPES buffer pH 7.5 + 100 mM KCl; (D) SEM picture of SPG electrodes; (E) Comparison of C1s XP spectra relative to a typical SPG prepared by varying curing time (0–180 s) and curing temperature (R.T.–180 °C).

Ca^{2+} cross-linked alginate hydrogel containing testing solution, as shown in figure 3(B). The corresponding CV in non-turnover conditions displayed no redox peaks in the voltage window investigated (figure 3(B), black curve). After substrate addition, the catalysis for D-glucose oxidation started at $E_{\text{ONSET}} = -0.068$ V with maximum current of 7 μA at $E = 0.4$ V (figure 3(B), red curve). In this case, the mass-transfer limitation is related to high roughness/porosity of hydrogel-based electrolyte, which allows to control the diffusion at the electrode surface.

The modified electrodes were tested in both liquid (figure 3(C), inset) and hydrogel-based electrolyte (figure 3(D), inset) by using amperometry increasing substrate concentration in the range 0–25 mM for D-glucose.

The calibration curve for PQQ-GDH/SPG electrodes in liquid electrolyte (spanning overall the 1×10^{-6} – 2.5×10^{-2} M), reported in figure 3(C), indicated a linear range from 10 μM to 2.5 mM (figure 3(C), inset), a detection limit of 3 ± 1 μM and a sensitivity of $1.7 \mu\text{A mM}^{-1}$ and a correlation coefficient of 0.99 (RSD 5.3%, $n = 10$). Additionally, the calibration curve was fitted to determine the classical Michaelis-Menten kinetic parameters, which resulted in I_{max} of $8.5 \pm 0.3 \mu\text{A}$ and an apparent Michaelis-Menten constant (K_M^{app}) of 2.2 ± 0.2 mM (similar to K_M measured in solution). The calibration curve for PQQ-GDH/SPG electrodes in hydrogel-based electrolyte reported in figure 3(D) (spanning overall the 1×10^{-6} – 2.5×10^{-2} M), indicated a linear range from 25 μM to 2.5 mM (figure 3(D), inset), a detection limit of $10 \pm 1 \mu\text{M}$ and sensitivity of $0.88 \mu\text{A mM}^{-1}$ and a correlation coefficient of 0.99 (RSD 5.4%, $n = 10$). The kinetic

parameters were determined as I_{max} of $8.1 \pm 0.4 \mu\text{A}$ and a K_M^{app} of 4.5 ± 0.6 mM (higher K_M than the ones measured in solution for homogeneous and heterogeneous catalysis). This can be ascribed to the porosity of hydrogel-based solid electrolyte, which affects the diffusion of the substrate towards the electrode.

The effects of pH and temperature on the proposed PQQ-GDH/SPG were evaluated in both cases, namely the liquid electrolyte and hydrogel-based electrolyte, and the results are shown in figures 3(E) and (F), respectively. Three different buffers have been tested, acetate, MOPS and HEPES buffer in order to cover the range of pHs between 3 and 10. The current signal increased with pH until 7.5, which corresponds to the maximum current signal obtained in HEPES buffer (figures 3(E) and (F)), by using either the liquid electrolyte or hydrogel-based electrolyte. 10 mM HEPES buffer pH 7.5 is therefore chosen for our experiments as an experimental condition closer to human physiological conditions. The optimum temperature in liquid electrolyte resulted to be 35 °C, as shown in figure 3(E). These results are in close agreement with the optimum pH and T values reported in literature for PQQ-GDH [36]. Similarly, the optimum temperature in hydrogel-based electrolyte resulted to be 30 °C, probably due to the instability of the hydrogel-based electrolyte at temperatures above that value [44].

The selectivity of PQQ-GDH/SPG electrode was studied in order to assess the influence of possible interfering compounds on its response. The signal obtained for a fixed concentration of D-glucose was compared to that obtained with equal amounts of interfering compounds such as D-fructose,

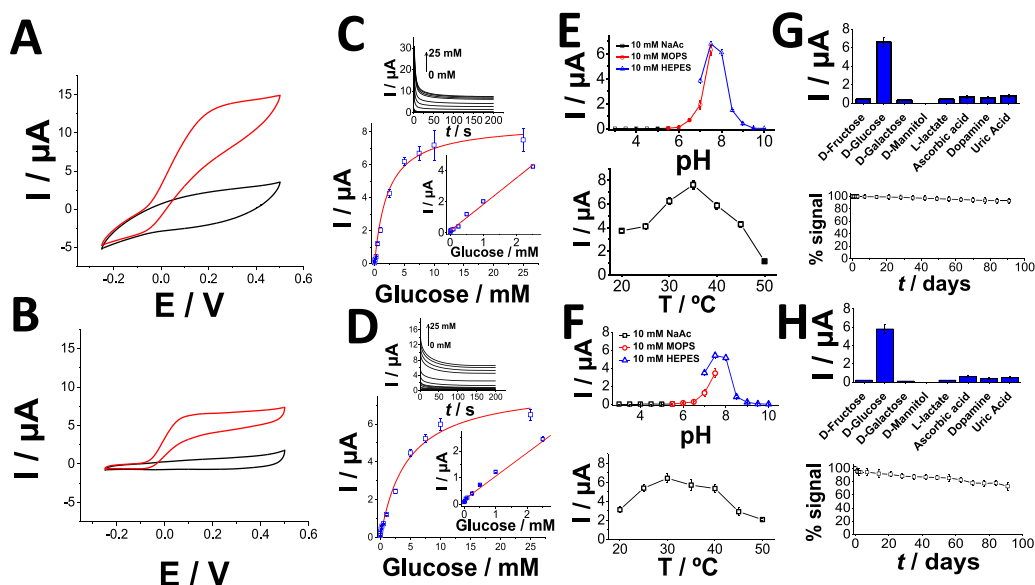


Figure 3. (A) CVs for PQQ-GDH/SPG electrode in non-turnover (10 mM buffer pH = 7.5 + 100 mM NaClO₄, black curve) and turnover conditions (addition of 10 mM D-glucose, red curve), scan rate 5 mV s⁻¹; (B) CVs for PQQ-GDH/SPG electrode with alginate hydrogel-based electrolyte in non-turnover (10 mM buffer pH = 7.5 + 100 mM NaClO₄, black curve) and turnover conditions (addition of 10 mM D-glucose, red curve), scan rate 5 mV s⁻¹; (C) Calibration curve for PQQ-GDH/SPG electrode in 10 mM buffer pH = 7.5 + 100 mM NaClO₄ based on the amperometric measurements performed at E_{appl} : +0.35 V by increasing substrate concentration in the range 0–25 mM for D-glucose—inset1: amperometry at E_{appl} : +0.35 V by increasing substrate concentration in the range 0–25 mM for D-glucose—inset2: linear range of calibration curve for PQQ-GDH/SPG electrode; (D) Calibration curve for PQQ-GDH/SPG electrode with alginate hydrogel-based electrolyte in 10 mM buffer pH = 7.5 + 100 mM NaClO₄ based on the amperometric measurements performed at E_{appl} : +0.35 V by increasing substrate concentration in the range 0–25 mM for D-glucose—inset1: amperometry at E_{appl} : +0.35 V by increasing substrate concentration in the range 0–25 mM for D-glucose—inset2: linear range of calibration curve for PQQ-GDH/SPG electrode; (E) Effect of different pHs and temperature on PQQ-GDH/SPG: 10 mM acetate buffer (black), 10 mM MOPS buffer (red) 10 mM HEPES buffer (blue). Experimental conditions: 10 mM D-glucose, applied potential + 0.35 V; (F) Effect of different pHs and temperature on PQQ-GDH/SPG with alginate hydrogel-based electrolyte: 10 mM acetate buffer (black), 10 mM MOPS buffer (red) 10 mM HEPES buffer (blue). Experimental conditions: 10 mM D-glucose, applied potential + 0.35 V; (G) Influence of interfering compounds on glucose response for PQQ-GDH/SPG: 500 μ M ascorbic acid, 500 μ M dopamine, 500 μ M D-fructose, 500 μ M D-mannitol, 500 μ M D-galactose, 500 μ M dopamine, 500 μ M uric acid and 10 mM D-glucose measured with amperometry at E_{appl} : +0.35 V and storage stability; (H) Influence of interfering compounds on glucose response for PQQ-GDH/SPG with alginate hydrogel-based electrolyte: 500 μ M ascorbic acid, 500 μ M dopamine, 500 μ M D-fructose, 500 μ M D-mannitol, 500 μ M D-galactose, 500 μ M dopamine, 500 μ M uric acid and 10 mM D-glucose measured with amperometry at E_{appl} : +0.35 V and storage stability.

D-galactose, D-mannitol, L-lactate, ascorbic acid, dopamine, and uric acid as shown in figures 3(G) and (H). No significant current responses were recorded except for ascorbic acid and uric acid, notably 10% and 12%, 8% and 6% of D-glucose signal in liquid and hydrogel-based electrolyte, respectively. In contrast to the other electrochemical interferents that were examined, ascorbic acid and uric acid display a notably higher diffusion coefficient ($D = 5.9 \times 10^{-6} \text{ cm}^2 \text{ s}^{-1}$ for ascorbic acid and $D = 7.5 \times 10^{-6} \text{ cm}^2 \text{ s}^{-1}$ for uric acid). Moreover, they exhibit easy oxidation at the electrode surface, specifically at the potential utilized for analytical measurements, whereas dopamine possesses a diffusion coefficient of $D = 8.2 \times 10^{-7} \text{ cm}^2 \text{ s}^{-1}$. The exceptional selectivity observed can be attributed to the relatively low operating potential of the third-generation electrode.

The storage stability of PQQ-GDH/SPG electrodes were investigated by monitoring the signal decrease of the current when the electrode is used for ten measurements every day over a period of 90 days for a 10 mM D-glucose solution, as reported in figures 3(G) and (H). The PQQ-GDH/SPG

electrodes showed a signal decrease of its initial response of less than 10% after 90 days by using a liquid electrolyte, and less than 20% by using a hydrogel-based electrolyte. This can be probably due to a combination of the intrinsic stability of the enzyme immobilized onto SPG electrodes as well as the porosity and stability of hydrogel-based electrolyte.

3.3. Bioelectrocatalytic characterization of BOx/SPG electrode

The electrocatalytic behavior of BOx/SPG was investigated in 10 mM HEPES buffer pH 7.5 + 100 mM NaClO₄, as liquid electrolyte and Ca²⁺ cross-linked alginate hydrogel containing testing solution by scanning the electrode in anaerobic conditions (figure 4(A), black curve) and in equilibrium with air (figure 4(A), red curve), respectively. Figure 4(B) (black curve) shows a CV recorded in anaerobic conditions in solution (not possible to perform with the hydrogel-based electrolyte) and with the hydrogel system in equilibrium with air (figure 4(B), red curve). From the conducted experiments,

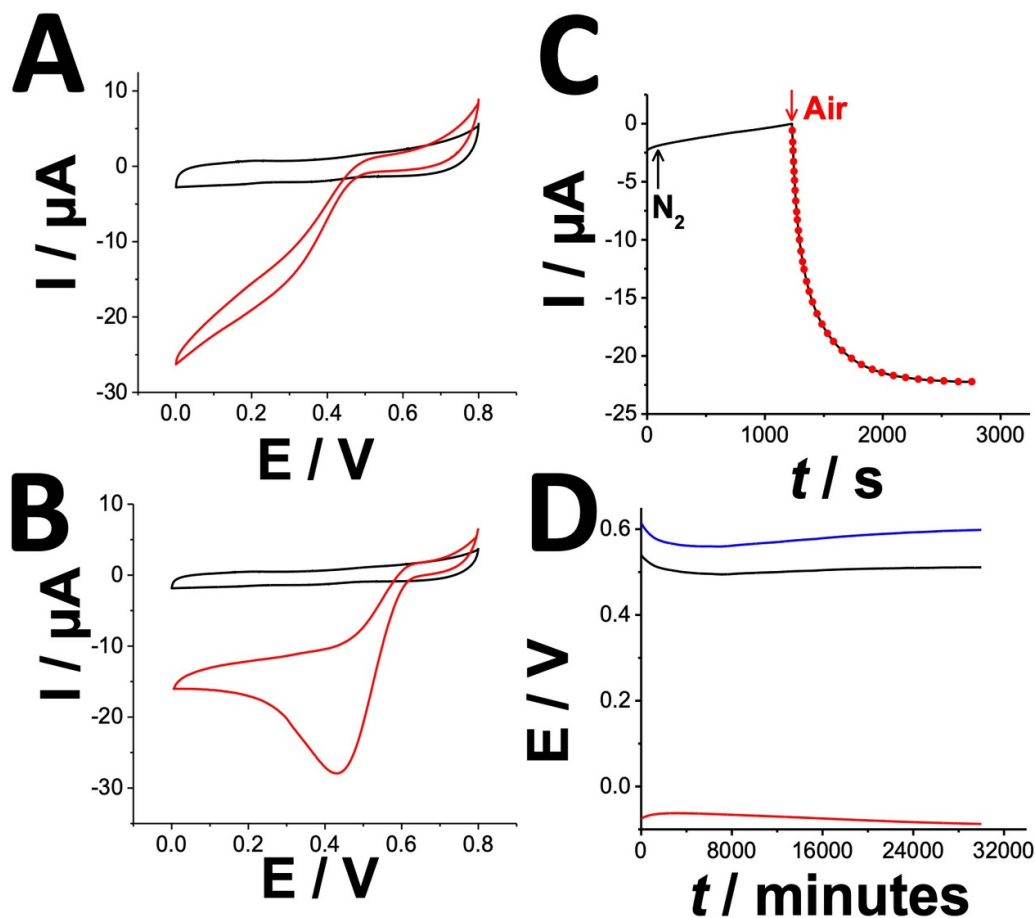


Figure 4. (A) CVs for BOx/SPG electrode in non-turnover (10 mM buffer pH = 7.5 + 100 mM NaClO₄, black curve) and turnover conditions (in equilibrium with air, red curve), scan rate 5 mV s⁻¹; (B) CVs for BOx/SPG electrode with alginate hydrogel-based electrolyte in non-turnover (10 mM buffer pH = 7.5 + 100 mM NaClO₄, black curve) and turnover conditions (in equilibrium with air, red curve), scan rate 5 mV s⁻¹; (C) Amperometry for BOx/SPG electrode in non-turnover (10 mM buffer pH = 7.5 + 100 mM NaClO₄, black line) and turnover conditions (in equilibrium with air, red dots) at E_{appl} : 0 V; (D) PQQ-GDH bioanode OCP (red line), BOx biocathode (black line) and OCV measurements for a single EFC (blue line) operating continuously over 500 h.

distinct electrocatalytic waves were observed, which can be primarily attributed electrostatic orientation of BOx near to its hydrophobic region adjacent to the T1 site. This specific arrangement enhances the DET reaction, resulting in an amplified electrocatalytic response. The catalytic curve, reported in figure 4(B), is mass-transfer limited probably due to the porosity of the hydrogel-based solid electrolyte where O₂ has lower diffusion rate compared to the liquid electrolyte.

To prove unequivocally the DET mechanism, BOx/SPG electrodes were analyzed by amperometry in anaerobic conditions (removing oxygen by purging nitrogen in solution) and in equilibrium with air, showing a current decrease to $22 \pm 1 \mu\text{A}$, as reported in figure 4(C). This highlights the biocatalytic ORR occurring at the enzyme modified electrode.

Before assembling the EFC with the hydrogel-based electrolyte, both the anode and cathode electrodes, namely PQQ-GDH/SPG and BOx/SPG, were characterized by open circuit potentiometry (OCP) to assess their individual operational stability over 500 h, as shown in figure 4(D) (anode: red curve

and cathode: black curve). In particular, PQQ-GDH/SPG electrodes showed an OCP of $-0.068 \pm 0.003 \text{ V}$ and BOx/SPG electrodes showed an OCP of $0.502 \pm 0.004 \text{ V}$, displaying an increased stability over 500 h, probably due to the porosity of the electrodes, which affects the amount of enzyme molecules immobilized and its stability. After assembling the EFC, the OCV resulted to be $0.562 \pm 0.002 \text{ V}$, which is in good agreement with the OCV that can be calculated as a difference between the OCP curves measured individually, namely 0.570 V.

3.4. Characterization of EFC assembled in series by using hydrogel-based electrolyte

Finally, the EFC was assembled with the hydrogel-based electrolyte reporting an OCV resulted to be $0.560 \pm 0.005 \text{ V}$, close to the theoretical difference between OCPs of bioanode and biocathode, figure 5(A).

A maximum power output of $5.9 \pm 0.6 \mu\text{W}$ at a cell voltage of 0.54 V was obtained, figure 5(A). The stability

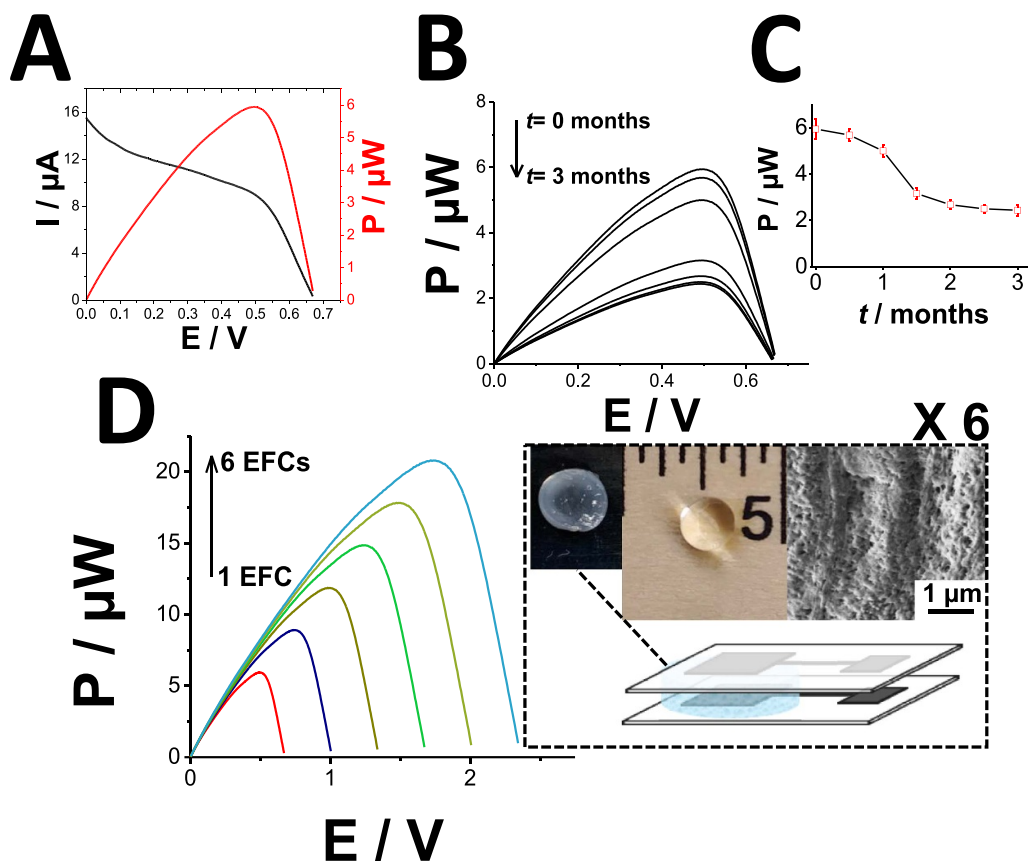


Figure 5. (A) Polarization (black curve) and Power output (red curve) curves for PQQ-GDH/SPG // SPG/BOx EFC in 10 mM D-glucose (prepared in 10 mM buffer pH = 7.5 + 100 mM NaClO₄), scan rate 1 mV s⁻¹; (B) Power output curves for PQQ-GDH/SPG // SPG/BOx EFC in 10 mM D-glucose (prepared in 10 mM buffer pH = 7.5 + 100 mM NaClO₄), scan rate 1 mV s⁻¹ recorded every 15 days; (C) Operational stability of for PQQ-GDH/SPG // SPG/BOx EFC; (D) Power output curves for six PQQ-GDH/SPG // SPG/BOx EFCs connected in series recorded in 10 mM D-glucose (prepared in 10 mM buffer pH = 7.5 + 100 mM NaClO₄), scan rate 1 mV s⁻¹ (insets: optical photos of hydrogel stacks and SEM picture).

of the EFC was further evaluated by running polarization curves every 15 days (for a total of 3 months) and measuring continuously the OCV over the same range of time, figures 5(B) and (C). After a month, the performance was decreasing in terms of both OCV (5%) and maximum power output (10%), respectively. The power output of a single EFC dropped to $2.4 \pm 0.1 \mu W$ after 3 months. This behavior can be mainly attributed to the progressive hydrogel and biocatalysts degradation. Moreover, the flexibility of EFC was assessed by bending the electrodes up to 50 times (figure S2) observing a 75% (in solution) and 68% (in the hydrogel-based electrolyte) of power output retaining.

Figure 5(D) reports the power output curve for the EFC assembled in series, up to EFCs. Considering 6 EFCs assembled in series in a stack-structure (like Voltaic pile), exhibiting an OCV of 2.36 ± 0.22 V with a maximum power output of $22.9 \pm 0.9 \mu W$ at a cell voltage of 1.95 V (operating in 10 mM D-glucose). Figure 5(D) reports also photos of

Ca²⁺ cross-linked alginate hydrogel stack and a SEM picture showing the porosity of the hydrogel layer.

A comparison of the results with those obtained by other researchers with EFCs based on GDH modified bioanodes and *Myrothecium verrucaria* BOx as biocathodes has been reported in table 1.

The power density output and OCV values obtained in our experiments consistently align with those reported in existing literature, indicating their comparability [46–50]. However, it is worth noting that there is a notable exception: an electrochemical FC (EFC) utilizing the combination of FADGDH/menadione/MWCNTs // Lac/MWCNTs achieved a power output of $799.36 \mu W cm^{-2}$. In our case, the relatively lower power output can be attributed to potential kinetic limitations in the interfacial electron transfer at both electrodes, as well as the stability of the enzyme layer. These factors likely contribute to the observed decrease in power generation efficiency.

Table 1. Comparison of potentially implantable hybrid glucose/oxygen EFCs. Abbreviations: 2-aminoanthracene diazonium salt (2-ANT), anthracene modified multiwalled-carbon nanotubes (AcMWCNTs), *Aspergillus niger* FAD-glucose dehydrogenase (*AnFADGDH*), *Burkholderia cepacia*n FAD-glucose dehydrogenase (*BcFADGDH*), FAD-glucose dehydrogenase (*FADGDH*), glassy carbon electrode (GCE), gold electrode (AuE), gold nanoparticles (AuNPs), laccase (Lac), linear polyethyleneimine modified with dimethylferrocene and separated by a three-carbon spacer (FcMe₂-C₃-LPEI), multi walled-carbon nanotubes (MWCNTs), *Myrothecium verrucaria* bilirubin oxidase (*MvBOx*), N-methyl-4(4'-formylstyryl)pyridinium methosulfate acetal (PVA-SbQ), 1,10-phenanthroline-5,6-dione (PLQ), polyMethylene Blue electropolymerized with 25 scans (pMB25), single walled-carbon nanotubes (SWCNTs), protoporphyrin IX (PP), stencil-printing graphite electrode (SPG), pyrrolo quinoline quinone glucose dehydrogenase (PQQ-GDH).

BFC	Conditions	OCV (V)	Power output	Operational stability	References
<i>BcFADGDH</i> /menadione/ MWCNTs <i>Lac</i> /MWCNTs	100 mM PBS buffer pH 7 containing 5 mM glucose	1.00	799.36 $\mu\text{W cm}^{-2}$ at 0.5 V	~15% drop in 100 h of continuous operation Half-life > 100 h	[46]
<i>FADGDH</i> /AuNPs composite-modified AuE <i>MvBOx</i> /SWCNTs/GCE	100 mM PBS buffer pH 7.4 containing 200 mM glucose	~ 0.5	~32.5 $\mu\text{W cm}^{-2}$ at 0.45 V	—	[47]
<i>FADGDH</i> /FcMe ₂ -C ₃ - LPEI/MWCNTs <i>MvBOx</i> /AcMWCNTs	200 mM PBS buffer pH 7.4 containing 5 mM glucose	0.60	35.4 $\mu\text{W cm}^{-2}$	~50% drop in 24 h of continuous operation	[48]
	200 mM PBS buffer pH 7.4 containing 100 mm glucose	0.60	100.4 $\mu\text{W cm}^{-2}$	—	
	Human serum	0.54	39.5 $\mu\text{W cm}^{-2}$	~60% drop in 24 h of continuous operation	
PVA-SbQ/ <i>AnFADGDH</i> / pMB25/MWCNTs <i>MvBOx</i> /2-ANT/MWCNTs	Single EFC: 50 mM PBS buffer pH 7.4 containing 5 mM glucose	0.78	25.8 $\mu\text{W cm}^{-2}$ at 0.57 V	Half-life > 24 h	
	Double-sided EFC: 50 mM PBS buffer pH 7.4 containing 5 mM glucose	0.78	31.0 $\mu\text{W cm}^{-2}$ at 0.57 V	—	[49]
	Double-sided EFC connected in series: 50 mM PBS buffer pH 7.4 containing 5 mM glucose	1.58	59.6 $\mu\text{W cm}^{-2}$ at 1.16 V	—	
	Double-sided EFC connected in series: human saliva	1.12	1.4 $\mu\text{W cm}^{-2}$ at 0.25 V	—	
	Double-sided EFC connected in series: artificial human serum	1.25	16.7 $\mu\text{W cm}^{-2}$ at 0.94 V	~40% drop in 24 h of continuous operation	
<i>FAD-GDH</i> / BP _{PLQ} BP _{PP} -BOx	McIlvaine buffer at pH 7.0 with 170 mM glucose	0.74	53 $\mu\text{W cm}^{-2}$	—	[50]
PQQ-GDH/SPG SPG/BOx	6 EFC with hydrogel-based stack: 10 mM HEPES buffer pH 7.5 containing 10 mM glucose	2.36	1.9 $\mu\text{W cm}^{-2}$ at 1.95 V (power density calculated considering 12 cm ² as electrode area)	~20% drop in 1 month of continuous operation	This work

4. Conclusions

In this study, we have successfully demonstrated the viability of efficient DET of PQQ-GDH and BOx enzymes on graphite stencil printed electrodes. We optimized and characterized two modified enzymatic electrodes to achieve optimal performance, which were then combined to assemble an EFC. Subsequently, to obtain an EFC with an OCV capable of powering small electronic devices like pacemakers or artificial pancreases, six EFCs

were connected in series using hydrogel-based electrolyte stacks.

The assembled biodevice was tested in a model solution containing 10 mM glucose, yielding promising results. The OCV obtained was 2.36 ± 0.22 V, with a maximum power output of 22.9 ± 0.9 μW at a cell voltage of 1.95 V. The relatively low maximum power output was primarily influenced by factors such as low electroactive area (4.05 ± 0.4 cm², which is typical for graphite electrodes), substrate diffusion through the hydrogel stack and

the presence of various interferents, leading to biofouling of the electrochemical surface. Moreover, the EFC activity over time is strongly affected by the decreasing enzymatic activity (~20% drop in 1 month of continuous operation).

To the best of our knowledge, this is the first report on the assembly of EFCs in series using stencil printed electrodes in combination with hydrogel stacks. This innovative approach represents a proof-of-concept towards the development of renewable power sources and could serve as a critical step in powering implantable bioelectronics, such as pacemakers.

Data availability statement

All data that support the findings of this study are included within the article.

Authors Contributions

P B conceived the project and wrote the manuscript. V M and A T performed all electrochemical measurements. N D performed XPS analyses. C D F and G S performed SEM measurements. L T, P B and E M directly supervised V M and A T during the project. L T is responsible for funding acquisition. L T, G S, E M and P B revised the manuscript. The final version was approved by all authors.

Conflict of interest

The authors declare no conflict of interest.

Funding

The following funding agencies are acknowledged: Biosensori analitici usa-e getta a base di transistori organici auto-alimentati per la rivelazione di biomarcatori proteomici alla singola molecola per la diagnostica decentrata dell'HIV (6CDD3786); Research for Innovation REFIN—Regione Puglia POR PUGLIA FESR-FSE 2014/2020; PMGB ARS01_01195; NoOne-A binary sensor with single-molecule digit to discriminate biofluids enclosing zero or at least one biomarker, ERC Stg2021, GA:101040383; PRIN project prot.2017RHX2E4 'At the forefront of Analytical Chemistry: disruptive detection technologies to improve food safety—ACTUaL'; IDF SHARID (ARS01_01270); CSGI is acknowledged for partial financial support.

ORCID iDs

Verdiana Marchianò  <https://orcid.org/0000-0002-7898-5394>

Angelo Tricase  <https://orcid.org/0000-0001-9976-2002>
Nicoletta Ditaranto  <https://orcid.org/0000-0001-7529-9906>

Eleonora Macchia  <https://orcid.org/0000-0002-1534-7336>

Cinzia Di Franco  <https://orcid.org/0000-0003-3310-7878>
Gaetano Scamarcio  <https://orcid.org/0000-0003-0808-4336>

Luisa Torsi  <https://orcid.org/0000-0002-0798-0780>

References

- [1] Bullen R A, Arnot T C, Lakeman J B and Walsh F C 2006 Biofuel cells and their development *Biosens. Bioelectron.* **21** 2015–45
- [2] Calabrese Barton S, Gallaway J and Atanassov P 2004 Enzymatic biofuel cells for implantable and microscale devices *Chem. Rev.* **104** 4867–86
- [3] Xiao X, Xia H, Wu R, Bai L, Yan L, Magner E, Cosnier S, Lojou E, Zhu Z and Liu A 2019 Tackling the challenges of enzymatic (bio) fuel cells *Chem. Rev.* **119** 9509–58
- [4] Santoro C, Bollella P, Erable B, Atanassov P and Pant D 2022 Oxygen reduction reaction electrocatalysis in neutral media for bioelectrochemical systems *Nat. Catal.* **5** 473–84
- [5] Shleev S 2017 Quo vadis, implanted fuel cell? *ChemPlusChem* **82** 522–39
- [6] Cadet M, Gounel S, Stines-Chaumeil C, Brilland X, Rouhana J, Louerat F and Mano N 2016 An enzymatic glucose/O₂ biofuel cell operating in human blood *Biosens. Bioelectron.* **83** 60–67
- [7] Falk M, Blum Z and Shleev S 2012 Direct electron transfer based enzymatic fuel cells *Electrochim. Acta* **82** 191–202
- [8] Meredith M T and Minter S D 2012 Biofuel cells: enhanced enzymatic bioelectrocatalysis *Annu. Rev. Anal. Chem.* **5** 157–79
- [9] Bollella P 2022 Enzyme-based amperometric biosensors: 60 years later... Quo vadis? *Anal. Chim. Acta* **1234** 340517
- [10] Katz E and Bollella P 2021 Fuel cells and biofuel cells: from past to perspectives *ISR J. Chem.* **61** 68–84
- [11] Solomon E I and Stahl S S 2018 *Introduction: Oxygen Reduction and Activation in Catalysis* (ACS Publications)
- [12] Lisdat F 2020 PQQ-GDH—Structure, function and application in bioelectrochemistry *Bioelectrochemistry* **134** 107496
- [13] Bandodkar A J and Wang J 2016 Wearable biofuel cells: a review *Electroanalysis* **28** 1188–200
- [14] Kim J, Kumar R, Bandodkar A J and Wang J 2017 Advanced materials for printed wearable electrochemical devices: a review *Adv. Electron. Mater.* **3** 1600260
- [15] Abreu C, Nedellec Y, Gross A J, Ondel O, Buret F, Goff A L, Holzinger M and Cosnier S 2017 Assembly and stacking of flow-through enzymatic bioelectrodes for high power glucose fuel cells *ACS Appl. Mater. Interfaces* **9** 23836–42
- [16] Silveri F *et al* 2023 Lab-made flexible third-generation fructose biosensors based on 0D-nanostructured transducers *Biosens. Bioelectron.* **237** 115450
- [17] Xie X, Guo R, Yang B, Li H, Yang F and Shen B 2021 Stencil-printed electrodes without current collectors and inactive additives on textiles for in-plane microsupercapacitors *J. Mater. Chem. A* **9** 25042–50
- [18] Kava A A and Henry C S 2021 Exploring carbon particle type and plasma treatment to improve electrochemical properties of stencil-printed carbon electrodes *Talanta* **221** 121553
- [19] Tricase A *et al* 2023 Water-based conductive ink formulations for enzyme-based wearable biosensors *Adv. Sens. Res.* **2300036**
- [20] Camargo J R *et al* 2021 Development of conductive inks for electrochemical sensors and biosensors *Microchem. J.* **164** 105998
- [21] Araujo D A, Camargo J R, Pradela-Filho L A, Lima A P, Muñoz R A A, Takeuchi R M, Janegitz B C and Santos A L 2020 A lab-made screen-printed electrode as a platform to study the effect of the size and functionalization of carbon

- nanotubes on the voltammetric determination of caffeic acid *Microchem. J.* **158** 105297
- [22] Camargo J R, Silva T A, Rivas G A and Janegitz B C 2022 Novel eco-friendly water-based conductive ink for the preparation of disposable screen-printed electrodes for sensing and biosensing applications *Electrochim. Acta* **409** 139968
- [23] Karagiannidis P G et al 2017 Microfluidization of graphite and formulation of graphene-based conductive inks *ACS Nano* **11** 2742–55
- [24] Mendez-Rossal H R and Wallner G M 2019 Printability and properties of conductive inks on primer-coated surfaces *Int. J. Polym. Sci.* **2019** e3874181
- [25] Bollella P and Gorton L 2018 Enzyme based amperometric biosensors *Curr. Opin. Electrochem.* **10** 157–73
- [26] Bollella P and Katz E 2020 Enzyme-based biosensors: tackling electron transfer issues *Sensors* **20** 3517
- [27] Cosnier S J, Gross A J, Le Goff A and Holzinger M 2016 Recent advances on enzymatic glucose/oxygen and hydrogen/oxygen biofuel cells: achievements and limitations *J. Power Sources* **325** 252–63
- [28] Chen Z, Yao Y, Lv T, Yang Y, Liu Y and Chen T 2022 Flexible and stretchable enzymatic biofuel cell with high performance enabled by textile electrodes and polymer hydrogel electrolyte *Nano Lett.* **22** 196–202
- [29] Yang Y, Su Y, Zhu X, Ye D, Chen R and Liao Q 2022 Flexible enzymatic biofuel cell based on 1, 4-naphthoquinone/MWCNT-modified bio-anode and polyvinyl alcohol hydrogel electrolyte *Biosens. Bioelectron.* **198** 113833
- [30] Xiao X 2022 The direct use of enzymatic biofuel cells as functional bioelectronics *eScience* **2** 1–9
- [31] Strakosas X, Huerta M, Donahue M J, Hama A, Pappa A M, Ferro M, Ramuz M, Rivnay J and Owens R M 2017 Catalytically enhanced organic transistors for in vitro toxicology monitoring through hydrogel entrapment of enzymes *J. Appl. Polym. Sci.* **134** 44813
- [32] Garland N T, Kaveti R and Bandodkar A J 2023 Biofluid-activated biofuel cells, batteries, and supercapacitors—a comprehensive review *Adv. Mater.* **2303197**
- [33] Miyake T, Haneda K, Yoshino S and Nishizawa M 2013 Flexible, layered biofuel cells *Biosens. Bioelectron.* **40** 45–49
- [34] Wu H, Zhang Y, Kjøniksen A-L, Zhou X and Zhou X 2021 Wearable biofuel cells: advances from fabrication to application *Adv. Funct. Mater.* **31** 2103976
- [35] Bollella P et al 2018 A glucose/oxygen enzymatic fuel cell based on gold nanoparticles modified graphene screen-printed electrode. Proof-of-concept in human saliva *Sens. Actuators B* **256** 921–30
- [36] Bollella P, Lee I, Blaauw D and Katz E 2020 A microelectronic sensor device powered by a small implantable biofuel cell *ChemPhysChem* **21** 120–8
- [37] Bartlett P N and Al-Lolage F A 2018 There is no evidence to support literature claims of direct electron transfer (DET) for native glucose oxidase (GOx) at carbon nanotubes or graphene *J. Electroanal. Chem.* **819** 26–37
- [38] Milton R D and Minter S D 2017 Direct enzymatic bioelectrocatalysis: differentiating between myth and reality *J. R. Soc. Interface* **14** 20170253
- [39] Rasmussen M, Abdellaoui S and Minter S D 2016 Enzymatic biofuel cells: 30 years of critical advancements *Biosens. Bioelectron.* **76** 91–102
- [40] Shleev S, Tkac J, Christenson A, Ruzgas T, Yaropolov A I, Whittaker J W and Gorton L 2005 Direct electron transfer between copper-containing proteins and electrodes *Biosens. Bioelectron.* **20** 2517–54
- [41] Roquero D M, Bollella P, Smutok O, Katz E and Melman A 2021 Protein release from interpenetrating polymer network hydrogels triggered by endogenous biomarkers *Mater. Today Chem.* **21** 100514
- [42] Massana Roquero D, Bollella P, Katz E and Melman A 2021 Controlling porosity of calcium alginate hydrogels by interpenetrating polyvinyl alcohol–diboronate polymer network *ACS Appl. Polym. Mater.* **3** 1499–507
- [43] Lavagnini I, Antiochia R and Magno F 2004 An extended method for the practical evaluation of the standard rate constant from cyclic voltammetric data *Electroanalysis* **16** 505–6
- [44] Kizling M, Biedul P, Zabost D, Stolarczyk K and Bilewicz R 2016 Application of hydroxyethyl methacrylate and ethylene glycol methacrylate phosphate copolymer as hydrogel electrolyte in enzymatic fuel cell *Electroanalysis* **28** 2444–51
- [45] Jia S, Wang Y, Xin G, Zhou S, Tian P and Zang J 2016 An efficient preparation of N-doped mesoporous carbon derived from milk powder for supercapacitors and fuel cells *Electrochim. Acta* **196** 527–34
- [46] Fapyane D, Lee S-J, Kang S-H, Lim D-H, Cho K-K, Nam T-H, Ahn J-P, Ahn J-H, Kim S-W and Chang I S 2013 High performance enzyme fuel cells using a genetically expressed FAD-dependent glucose dehydrogenase α -subunit of Burkholderia cepacia immobilized in a carbon nanotube electrode for low glucose conditions *Phys. Chem. Chem. Phys.* **15** 9508–12
- [47] Yehezkeili O, Tel-Vered R, Raichlin S and Willner I 2011 Nano-engineered flavin-dependent glucose dehydrogenase/gold nanoparticle-modified electrodes for glucose sensing and biofuel cell applications *ACS Nano* **5** 2385–91
- [48] Milton R D, Lim K, Hickey D P and Minter S D 2015 Employing FAD-dependent glucose dehydrogenase within a glucose/oxygen enzymatic fuel cell operating in human serum *Bioelectrochemistry* **106** 56–63
- [49] Zumpano R, Lambertini L, Tortolini C, Bollella P, Favero G, Antiochia R and Mazzei F 2020 A glucose/oxygen enzymatic fuel cell exceeding 1.5 V based on glucose dehydrogenase immobilized onto polyMethylene blue-carbon nanotubes modified double-sided screen printed electrodes: proof-of-concept in human serum and saliva *J. Power Sources* **476** 228615
- [50] Gross A J, Chen X, Giroud F, Abreu C, Le Goff A, Holzinger M and Cosnier S 2017 A high power buckypaper biofuel cell: exploiting 1,10-Phenanthroline-5,6-dione with FAD-dependent dehydrogenase for catalytically-powerful glucose oxidation *ACS Catal.* **7** 4408–16